UNDER REVIEW

RESCIENCE C

Replication / Ecology

[Re] Reproductive pair correlations and the clustering of organisms

Coralie Picoche[1,2] and Frederic Barraquand[1,2]

[1]Institute of Mathematics of Bordeaux, CNRS University of Bordeaux, Talence, France – [2]Integrative and Theoretical Ecology, LabEx COTE, University of Bordeaux, Pessac, France

Edited by
(Editor)

Received
01 November 2018

Published
19 February 2021

DOI
–

Introduction

In the present work, we attempt to replicate the results of Young et al. 2001 "Reproductive pair correlations and the clustering of organisms" [1], an analysis of the clustering of organisms in an homogeneous environment mimicking marine turbulence. Using an individual-based model of independent, random-walking particles (also called "brownian bugs"), they show that simple ecological processes such as birth and death in a turbulent and viscous flow leads to the formation of elongated aggregates and therefore departure from the usual, homogeneous solution of the advection-diffusion-reaction equation for a large population. This could explain the observed patchiness of communities such as the phytoplankton.

Our first interest in this paper was mostly driven by a major ecological question: the so-called paradox of the plankton [2], i.e. the surprising diversity of phytoplankton species competing for the same resources in a seemingly homogeneous environment. Aggregation of phytoplanktonic organisms, observed at macro- to micro-scales [3, 4], could explain part of their coexistence, as spatial clustering can help reduce interspecific interactions [5] and/or allow species to benefit from different organic substrates [6]. Due to their size, microphytoplankton organisms experience a mostly viscous environment in a laminar shear fields, with random, but homogeneous changes in directions due to turbulence [7]. Ecological phenomena as simple as growth and death, which occur at the phytoplankton scale, interact with these hydrodynamics processes and can lead to aggregates. In this context, a better understanding of the interactions between demographic stochasticity and environmental fluctuations at small scales could provide further explanation for the distribution and coexistence of these organisms in turbulent environments.

In this replication, we aim not only to replicate the main results of the paper, but also to clarify and develop the mathematical background behind the main equations governing the dynamics of the model.

Correspondence should be addressed to Coralie Picoche (coralie.picoche@u-bordeaux.fr)
The authors have declared that no competing interests exist.
Code is available at https://github.com/CoraliePicoche/brownian_bug_fluid/code..

Methods

Brownian bug model

The brownian bug model is a discrete-time, individual-based model, here presented in its 2D formulation. Each particle is characterized by the vector of its Cartesian coordinates $\boldsymbol{x} = \begin{pmatrix} x_1 \\ x_2 \end{pmatrix}$ and its original position on the y-axis at $t = 0$ (a child particle inherits this attribute), this last attribute being used only for representation purposes. Space is a $L \times L$ square with periodic boundary conditions. Each timestep, of duration τ, is divided into three substeps: (1) demographic processes, (2) diffusion, and (3) advection.

(1) The first substep is a Galton-Watson branching process. Each organism has a fixed probability (p) of reproducing, dying (q), or remaining unchanged ($1 - p - q$). When an individual reproduces, a new organism appears on top of the parent. In this paper, $p = q = 0.5$.
(2) Diffusion is modeled as a brownian motion, i.e. $\boldsymbol{x'}_k(t) = \boldsymbol{x}(t) + \delta\boldsymbol{x}(t)$ where each component of $\delta\boldsymbol{x}(t)$ follows a Gaussian distribution $(0, \Delta)$ where $D = \frac{\Delta^2}{2\tau}$ is the diffusivity.
(3) The turbulent flow governing advective stirring follows the Pierrehumbert random map.

$$x_1(t+\tau) = x'_1(t) + (U\tau/2)\cos[kx'_2(t) + \phi(t)] \quad (1)$$
$$x_2(t+\tau) = x'_2(t) + (U\tau/2)\cos[kx_1(t+\tau) + \theta(t)] \quad (2)$$

where $\phi(t)$ and $\theta(t)$ are random phases uniformly distributed between 0 and 2π, $k = 2\pi/L$ and U is the stretching parameter.

Unless otherwise specified, each simulation is initialized with $N_0 = 20,000$ particles uniformly distributed in a 1×1 square and run for 1000 timesteps.

Relation with the advection-diffusion-reaction approximation

In continuous time, the distribution of particles in conditions similar as those described in the brownian bug model can be approximated by the advection-diffusion-reaction (ADR) equation.

$$\frac{dC}{dt} = D\nabla^2 C + (\lambda - \mu)C \quad (3)$$

where C is the concentration of particles, λ is the growth rate ($\lambda = p/\tau$) and μ is the death rate ($\mu = q/\tau$). When $\lambda = \mu$, the solution of eq. 3 is $C(\boldsymbol{x}, t) = C_0$ where C_0 is the initial uniform concentration. To compare this theoretical distribution to the actual distribution, the brownian bug model is run without the advection component ($U = 0$).

To assess the effect of the turbulent motion, the model is also run without its demographic component, but with advection and diffusion.

Pair correlation function G(r,t)

The pair correlation function (hereafter, pcf) $G(\boldsymbol{x}_i, \boldsymbol{x}_j, t)$ is defined so that $G(\boldsymbol{x}_i, \boldsymbol{x}_j, t)dA_1dA_2$ is the probability finding a pair of brownian bugs with one member in the area dA_1 around $\boldsymbol{x}_1$ and the other in the area dA_2 around $\boldsymbol{x}_2$. The radial density function $g(r, t)$ is defined as $G(\boldsymbol{x}_i, \boldsymbol{x}_j, t) = C^2 g(r, t)$ with $r = |\boldsymbol{x}_i - \boldsymbol{x}_j|$. As the pair correlation disappear when $r \to \infty$, $g \to 1$.

We should note here that these notations differ from usual notations (see, e.g., [8]): pcf may correspond to g while G is defined as the pair density. We will keep the notations of [1] hereafter.

Derivation of G(r,t) — Finding back Eq. (2) in the original paper?

$$\frac{\partial G}{\partial t} = 2Dr^{1-d}\frac{\partial}{\partial r}\left(r^{d-1}\frac{\partial G}{\partial r}\right) + 2(\lambda-\mu)G + \gamma r^{1-d}\frac{\partial}{\partial r}\left(r^{d+1}\frac{\partial G}{\partial r}\right) + 2\lambda C\delta(\boldsymbol{x}) \quad (4)$$

where $\boldsymbol{x}$ is the position of the particle.

We focus on the case $d = 2$ and $\lambda = \mu$, which means Eq. (4) can be reduced to

$$\frac{\partial G}{\partial t} = \frac{2D}{r}\frac{\partial}{\partial r}\left(r\frac{\partial G}{\partial r}\right) + \frac{\gamma}{r}\frac{\partial}{\partial r}\left(r^3\frac{\partial G}{\partial r}\right) + 2\lambda C\delta(\boldsymbol{x}) \quad (5)$$

The value of γ is computed from simulations (see SI.)

Analytical solution with advection — In the presence of advection ($\gamma \neq 0$), a steady-state solution can be found.

$$\begin{aligned}
\frac{2D}{r}\frac{\partial}{\partial r}\left(r\frac{\partial G}{\partial r}\right) + \frac{\gamma}{r}\frac{\partial}{\partial r}\left(r^3\frac{\partial G}{\partial r}\right) + 2\lambda C\delta(\boldsymbol{x}) &= 0 \\
\Leftrightarrow 2\pi r\left(\frac{2D}{r}\frac{\partial}{\partial r}\left(r\frac{\partial G}{\partial r}\right) + \frac{\gamma}{r}\frac{\partial}{\partial r}\left(r^3\frac{\partial G}{\partial r}\right) + 2\lambda C\delta(\boldsymbol{x})\right) &= 0 \\
\Leftrightarrow 2\pi\left(2D\frac{\partial}{\partial r}\left(r\frac{\partial G}{\partial r}\right) + \gamma\frac{\partial}{\partial r}\left(r^3\frac{\partial G}{\partial r}\right)\right) + 2\pi r 2\lambda C\delta(\boldsymbol{x}) &= 0 \quad (6)
\end{aligned}$$

We can then integrate Eq. (6) over a small area centered on a particle, with radius ρ. Let us first note that

$$\begin{aligned}
\int_{R^2}\delta(\boldsymbol{x})d^2\boldsymbol{x} &= 1 \\
\Leftrightarrow \int_0^{2\pi}\int_0^{\rho}\delta(r')\delta(\theta)r'dr'd\theta &= 1 \\
\Leftrightarrow 2\pi\int_0^{\rho}\delta(\boldsymbol{x'})r'dr' &= 1 \quad (7)
\end{aligned}$$

Using Eq. (6) and (7), we can integrate between 0 and ρ,

$$\begin{aligned}
0 &= 2\pi\left(2D\rho\frac{\partial G}{\partial r} + \gamma\rho^3\frac{\partial G}{\partial r}\right) + 2\lambda C \\
\Leftrightarrow \quad \frac{\partial G}{\partial r} &= -\frac{1}{2\pi}\frac{2\lambda C}{2D\rho + \gamma\rho^3} \quad (8)
\end{aligned}$$

Eq. (8) can now be integrated between ρ and ∞, knowing that $G(\infty) = C^2$.

$$C^2 - G(\rho) = -\frac{1}{2\pi}\int_{\rho}^{\infty}\frac{2\lambda C}{2Dr + \gamma r^3}dr \quad (9)$$

Using the variable change $u = 2Dr + \gamma r^3$, the integral is equivalent to $\int \frac{u'}{u}du$.

$$C^2 - G(\rho) = -\frac{\lambda C}{2\pi}\frac{1}{4D}[\log(\gamma) - \log(\frac{2D}{r^2} + \gamma)] \quad (10)$$

$$\Leftrightarrow G(\rho) = \frac{\lambda C}{8\pi D}\log\left(\frac{2D + \gamma r^2}{\gamma r^2}\right) + C^2 \quad (11)$$

Finally, the pair correlation function $g = G/C^2$ is defined as

$$g = \frac{\lambda}{8\pi DC}\log\left(\frac{2D + \gamma r^2}{\gamma r^2}\right) + 1 \quad (12)$$

Analytical solution without advection — When $U = 0$, $\gamma = 0$ and there is no steady solution. We can get back to Eq. (5).

$$\frac{\partial G}{\partial t} = \frac{2D}{r}\frac{\partial}{\partial r}\left(r\frac{\partial G}{\partial r}\right) + 2\lambda C\delta(\boldsymbol{x}) \quad (13)$$

Assuming an isotropic environment (and switching to the polar coordinate system), this means

$$\frac{\partial G}{\partial t} - 2D\Delta G = 2\lambda C\delta(\boldsymbol{x}) \quad (14)$$

where $\Delta = \nabla^2$ is the Laplacian operator.

We therefore have

$$\mathcal{L}G(\boldsymbol{x}, t) = 2\lambda C\delta(\boldsymbol{x}) \quad (15)$$

where $\mathcal{L}$ is the linear differential operator $\partial_t - 2D\Delta$.

We can use the Green's function H, defined with $\mathcal{L}H = \delta(\boldsymbol{x}, t) = \delta(\boldsymbol{x})\delta(t)$.

By definition, we know that $G(y) = \int H(y, s)2\lambda C\delta(s)ds$ (where $y = (\boldsymbol{x}, t)$) is a solution to Eq.(15).

$$G(\boldsymbol{x}, t) = 2\lambda C\int_{R^2}\int_0^t H(\boldsymbol{x} - \boldsymbol{x}', t')\delta(\boldsymbol{x}')d^2\boldsymbol{x}'dt'$$

$$\Leftrightarrow = 2\lambda C\int_0^t H(\boldsymbol{x}, t')dt' \quad (16)$$

Eq.(16) can be used in Eq. (13):

$$\begin{aligned}
&\frac{\partial}{\partial t}\left(2\lambda C\int_0^t H(\boldsymbol{x}, t')dt'\right) &&= 2D2\lambda C\Delta\int_0^t H(\boldsymbol{x}, t')dt' + 2\lambda C\delta(\boldsymbol{x})\\
\Leftrightarrow &\int_0^t\left(\frac{\partial H(\boldsymbol{x}, t')}{\partial t'} - 2D\Delta H(\boldsymbol{x}, t')\right)dt' &&= \delta(\boldsymbol{x})\\
\Leftrightarrow &\int_0^t \delta(\boldsymbol{x})\delta(t')dt' &&= \delta(\boldsymbol{x})
\end{aligned}$$

which is true.

A solution for the Green's function using $\mathcal{L} = \partial_t - 2D\Delta$ in 2 dimensions is

$$H(r, t) = \frac{1}{4\pi 2Dt}\exp(\frac{-r^2}{4 \times 2Dt})$$

.
$G(r,t)$ can then be computed:

$$G(r,t) = 2\lambda C \left[\frac{E1\left(\frac{r^2}{8Dt'}\right)}{8D\pi} \right]_0^t \tag{17}$$

where $E1$ is the exponential integral. Using $G(r,0) = C^2$ and $\lim_{x\to+\infty} E1 = 0$ in Eq. (17),

$$G(r,t) = 2\lambda C \frac{E1\left(\frac{r^2}{8Dt}\right)}{8D\pi} + C^2 \tag{18}$$

$$\Leftrightarrow g(r,t) = \frac{2\lambda}{C} \frac{E1\left(\frac{r^2}{8Dt}\right)}{8D\pi} + 1 \tag{19}$$

Results

We were able to reproduce the spatial distributions of brownian bugs in each case described in [1].

We can see in Fig. 1 the clumping of organisms which illustrates the failure of the ADR approximation at small scales due to demographic processes. Fig. 2 also show that hydrodynamics alone cannot ensure cluster formation.

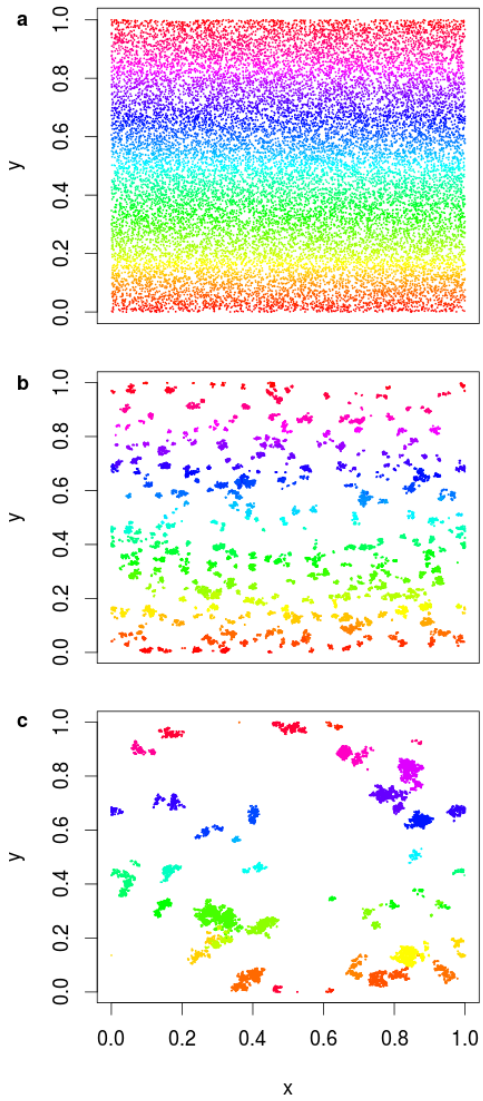

Figure 1. Distribution of brownian bugs at different times in a simulation with $\Delta = 10^{-3}$ and $U = 0$: initial conditions with a Poisson spatial distribution (a), $t = 100\tau$ (b) and $t = 1000\tau$ (c). Each particle is identified by a color which corresponds to the initial position on the y axis of its ancestor at t=0.

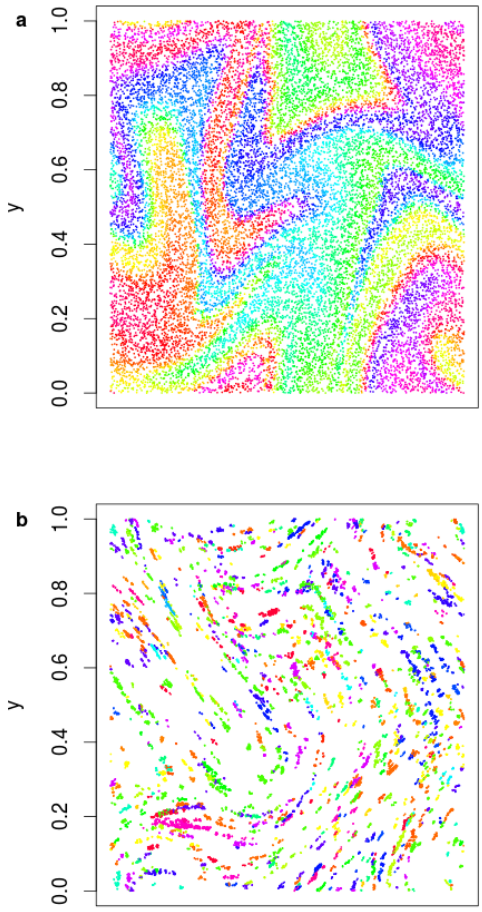

Figure 2. Distribution of brownian bugs with different processes in a simulation with $\Delta = 10^{-3}$ and $U\tau/2 = 0.1$: without demographic processes at $t = 30\tau$ (a), and with demographic processes $t = 1000\tau$ (b). Each particle is identified by a color which corresponds to the initial position on the y axis of its ancestor at t=0.

Fig. 3 proved much more challenging. Retrieving the analytical solutions of eq. 5 was the most difficult. However, we also encountered issues when computing the pair correlation functions on simulations: for large values of r/Δ, the pcf was set to 0 due to sampling issue. With the same initial conditions as the previous simulations, i.e. $N_0 = 20,000$ particles uniformly distributed in a 1×1 square (the size shown in the two previous figures), there were too many missing values to assess the fit of the simulation to the theory. We therefore chose to increase the number of particles to $N_0 = 200,000$ over an area of 10. We can see on Fig. 3 that there are still missng values but that we can confirm that simulated and analytical pcf match.

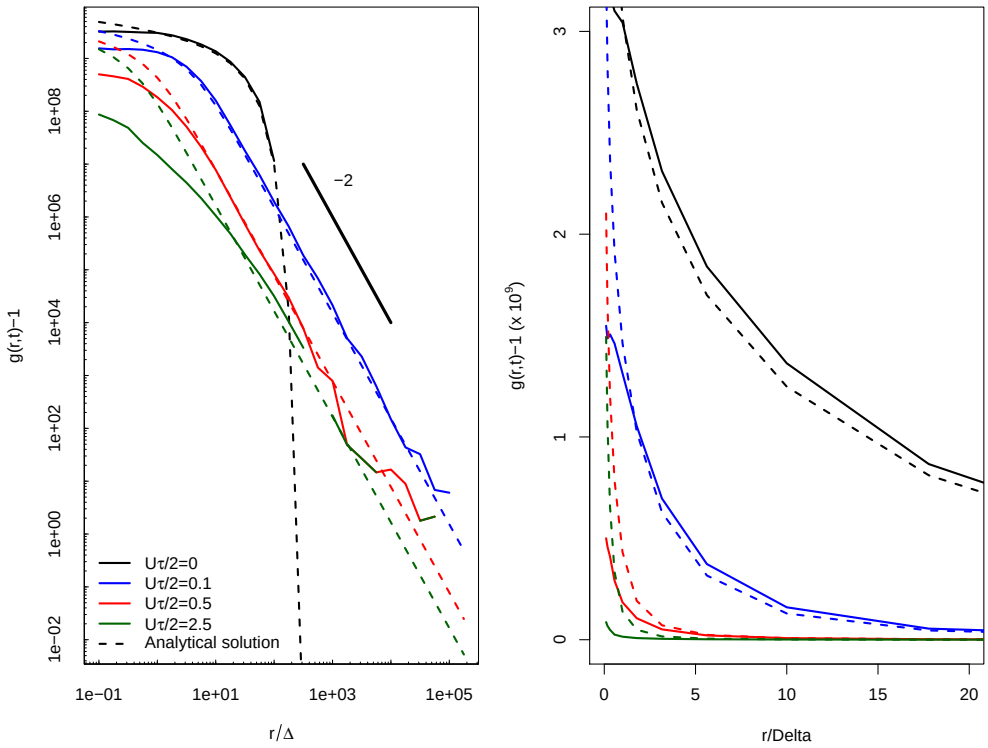

Figure 3. Logarithmic (a) and linear (b) plots of $g(r,t)$ versus r/Δ, with $\Delta = 10^{-7}$ and $U\tau/2 = 0, 0.1, 0.5, 2.5$ at $t = 1000\tau$. Solide lines result from simulations, dotted lines correspond to analytical solutions and the solid grey line indicates the r^{-2} scaling predicted by eq. 4.

Discussion

We successfully replicated both the simulations and retrieved the analytical solutions of [1]. Even though stochasticity prevents us from replicating exactly the same distributions as those seen in Fig. 1 and Fig. 2, we considered the patterns to be close enough to validate the simulations. Fig. 3 was also very close to the one shown in the article, even though we encountered some sampling issues probably due to the number of particles we used. Even though we used the number indicated in the legend of the original Fig. 3, William Young, the first author of the article confirmed that a higher number of particles might work better and might have been used for this figure.

The most challenging part of the replication was not actually to replicate the results, but to find the analytical expression of the pair density function $G(r,t)$. In the absence of additional explanations regarding both the derivation and the solution for this function, we could not compute the analytical solutions shown in Fig. 3. William Young helped us find back these solutions, with quick and frequent feedbacks. We hope that the additional details on the theory will help the reader through the article.

The original paper was not strongly quantitative; we thus wondered about the time and spatial scales that could be used for a realistic phytoplankton model. The length of the square side, L, is defined as the Kolmogorv scale, that is the scale at which viscosity starts dominating turbulence. In the ocean, this value oscillates between 1 and 10 mm [9] (which corresponds to the value which was given by William Young, i.e. 1 cm). If we consider a phytoplankton doubling rate of 0.5-1 d^{-1} [10], $p = 0.5$ means that

$\tau = 0.25 - 0.5$ d. In this case, assuming we can write $U\tau/2 = 0.1L$ (the value used in Fig. 2), $U \approx 5.5\ 10^{-5}$ cm.s^{-1}, which seems very low for the oceanic current (around 1-10 cm.s^{-1} near the coast in [5], similar in the North Atlantic Ocean [11]). We should therefore have a lower reproduction probability p, if we wanted to keep the values of the other parameters. The diffusion coefficient can be hard to approximate. Broström [12] suggests a value of 10^{-8} m^2.s^{-1}, which would lead to $\Delta \approx 10^{-4}$. This is much higher from the value used in Fig. 3 (10^{-7}) but only one order of magnitude lower than the value used in Fig. 1 and Fig. 2. A thorough discussion of the parameters is therefore necessary before extrapolating these results to real phytoplanktoni systems.

As the brownian bug model is very general, a next step would be to consider similar dynamics in a 3D-model, for which the pair correlation function can be evaluated easily. Using actual concentrations of phytoplanktonic organisms, between 10^3 and 10^6 C/L, this would lead to 1 to 10^3 organisms if we kept L = 1 cm. We may therefore need to increase the size of the considered square if doing so. With a more quantitative models, this could allow a new modeling of phytoplanktonic organisms.

Acknoweldgements

We are very grateful to William Young for his help through the theoretical part of Young et al. 2001.

References

1. W. R. Young, A. J. Roberts, and G. Stuhne. “Reproductive pair correlations and the clustering of organisms.” In: **Nature** 412.6844 (2001), pp. 328–331.
2. G. E. Hutchinson. “The paradox of the plankton.” In: **The American Naturalist** 95.882 (1961), pp. 137–145.
3. S. Lovejoy. “Universal multifractals and ocean patchiness: phytoplankton, physical fields and coastal heterogeneity.” In: **Journal of Plankton Research** 23.2 (2001), pp. 117–141.
4. B. Pinel-Alloul and A. Ghadouani. “Spatial heterogeneity of planktonic microorganisms in aquatic systems.” In: **The spatial distribution of microbes in the environment**. Springer, 2007, pp. 203–310.
5. J. S. Font-Muñoz, A. Jordi, I. Tuval, J. Arrieta, S. Anglès, and G. Basterretxea. “Advection by ocean currents modifies phytoplankton size structure.” In: **J. R. Soc. Interface** 14.130 (2017), p. 20170046.
6. J. R. Seymour, Marcos, and R. Stocker. “Resource Patch Formation and Exploitation throughout the Marine Microbial Food Web.” In: **The American Naturalist** 173.1 (2009), p. 15.
7. F. Peters and C. Marrasé. “Effects of turbulence on plankton: an overview of experimental evidence and some theoretical considerations.” In: **Marine Ecology Progress Series** 205 (2000), pp. 291–306.
8. J. Illian, A. Penttinen, H. Stoyan, and D. Stoyan. **Statistical analysis and modelling of spatial point patterns**. Vol. 70. John Wiley & Sons, 2008.
9. A. D. Barton, B. A. Ward, R. G. Williams, and M. J. Follows. “The impact of fine-scale turbulence on phytoplankton community structure.” In: **Limnology and Oceanography: Fluids and Environments** 4.1 (2014), pp. 34–49.
10. J. E. Bissinger, D. J. S. Montagnes, J. Harples, and D. Atkinson. “Predicting marine phytoplankton maximum growth rates from temperature: Improving on the Eppley curve using quantile regression.” In: **Limnology and Oceanography** 53.2 (2008), pp. 487–493.
11. M. K. Flatau, L. Talley, and P. P. Niiler. “The North Atlantic Oscillation, Surface Current Velocities, and SST Changes in the Subpolar North Atlantic.” In: **Journal of Climate** 16.14 (2003), pp. 2355–2369.
12. G. Broström. “On advection and diffusion of plankton in coarse resolution ocean models.” In: **Journal of Marine Systems** 35.1-2 (2002), pp. 99–110.

Supplementary Material

Stretching parameter γ

γ is computed with simulations, with the formula $r(t) \propto exp(\gamma dt) \rightarrow \frac{1}{2}ln(r(t)) = \gamma t$ if $d = 2$ with r being the separation between pairs of particles. γ is estimated as the slope of

$$\frac{1}{2}\langle ln(r(t))\rangle = f(t)$$

with $\langle ln(r(t))\rangle$ being the average obtained from 800 pairs of particles.

$$\forall t, \langle ln(r(t))\rangle = \frac{1}{800}\sum_{p=1}^{800} ln(r(\boldsymbol{x}_{1,p}(t) - \boldsymbol{x}_{2,p}(t)))$$

where $r(\boldsymbol{x}_{1p}(t) - \boldsymbol{x}_{2p}(t))$ is the distance between a particle $1p$ at position $\boldsymbol{x}_{1p}$ and its counterpart $2p$, initialized with $r(0) = 10^{-7}\forall p$ (see Fig. 4 for γ estimates).

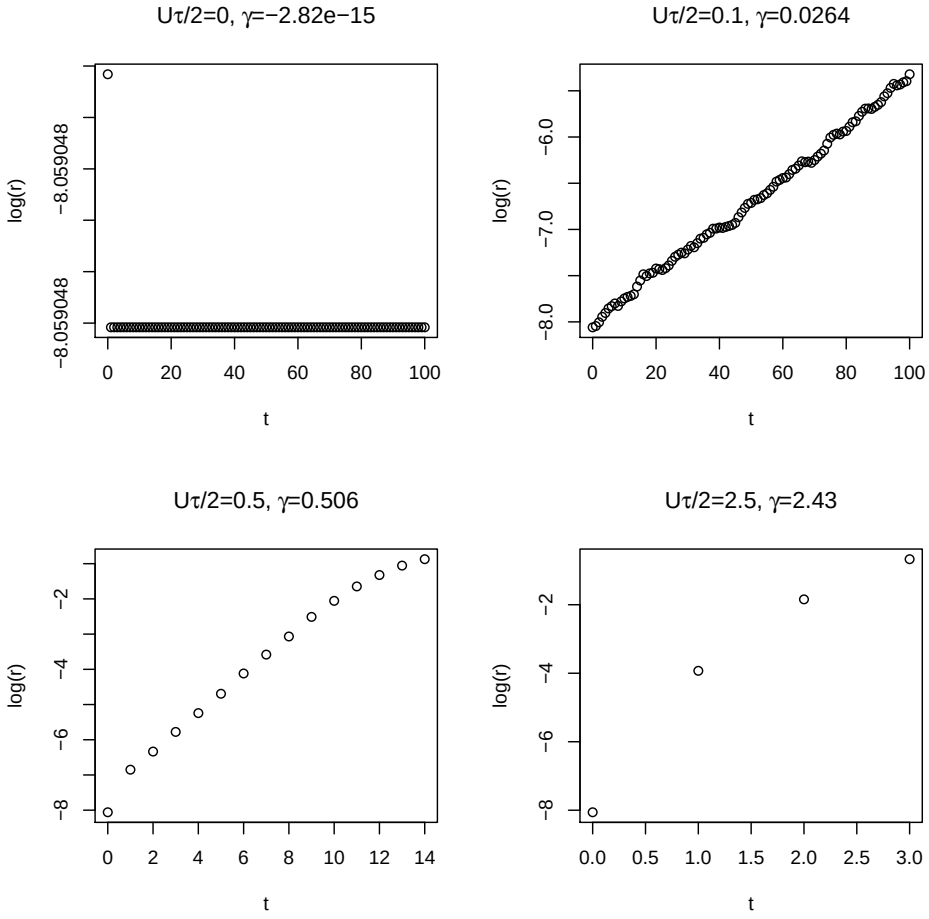

Figure 4. Estimates of γ for different $U\tau/2$